Inclined nanoimprinting lithography for 3D nanopatterning

2011 Nanotechnology 22 225302

(http://iopscience.iop.org/0957-4484/22/22/225302)

Nanotechnology **22** (2011) 225302 (8pp) doi:10.1088/0957-4484/22/22/225302

Inclined nanoimprinting lithography for 3D nanopatterning

Zhan Liu[1,3], **David G Bucknall**[1] **and Mark G Allen**[2]

[1] School of Materials Science and Engineering, Georgia Institute of Technology, Atlanta, GA 30332, USA
[2] School of Electrical and Computer Engineering, Georgia Institute of Technology, Atlanta, GA 30332, USA

E-mail: zhan.liu@gatech.edu

Received 24 January 2011, in final form 6 March 2011
Published 4 April 2011
Online at stacks.iop.org/Nano/22/225302

Abstract

We report a non-conventional shear-force-driven nanofabrication approach, inclined nanoimprint lithography (INIL), for producing 3D nanostructures of varying heights on planar substrates in a single imprinting step. Such 3D nanostructures are fabricated by exploiting polymer anisotropic dewetting where the degree of anisotropy can be controlled by the magnitude of the inclination angle. The feature size is reduced from micron scale of the template to a resultant nanoscale pattern. The underlying INIL mechanism is investigated both experimentally and theoretically. The results indicate that the shear force generated at a non-zero inclination angle induced by the INIL apparatus essentially leads to asymmetry in the polymer flow direction ultimately resulting in 3D nanopatterns with different heights. INIL removes the requirements in conventional nanolithography of either utilizing 3D templates or using multiple lithographic steps. This technique enables various 3D nanoscale devices including angle-resolved photonic and plasmonic crystals to be fabricated.

(Some figures in this article are in colour only in the electronic version)

1. Introduction

The capability to fabricate 3D nanostructures with multiple heights is a significant technical driver with various applications in integrated photonics, plasmonics, micro- and nanofluidics, nanobiochemistry, nanotribology as well as nanoelectromechanical systems (NEMS) [1]. To these ends, nanoimprinting lithography (NIL) [2–5] and soft lithography [6–11] have been recently exploited due to their ability to form the desired structures in a convenient manner with the potential of low cost and high throughput. However, to create structures with variable topographic feature heights using these methods would require either templates with 3D nanostructures over a large area for direct 3D nanoimprinting, or the ability to perform precise registration and alignment between the templates and substrates to repetitively transfer 2D structures. These factors inevitably increase the fabrication difficulties and process complexities.

Recently we proposed a convenient and inexpensive nanofabrication approach, inclined nanoimprinting lithography (INIL), for producing 3D nanopatterns of varying heights in a single imprinting step by utilizing an inclined poly(dimethylsiloxane) (PDMS) mold with 1D/2D microscopic patterned structures [12]. INIL derives from the anisotropic dewetting process of polymer thin films [8, 13], augmented by the observation that the degree of anisotropy can be controlled by the angle of inclination of the system. Although observation of the effect was described in [12], no explanation of the underlying mechanism or description of the limits of applicability was given.

In this work the underlying mechanism of INIL is described both theoretically and experimentally. Nanolithography polymer resist ZEP520 [14], poly(methyl-α-chloroacrylate-*co*-α-methylstyrene), is used as the imprinting resist due to its more amenable material properties for post-INIL process applications, such as reactive ion dry etching compatibility for 3D nanopattern transfer. This developed INIL technique not only maintains the high throughput advantages

[3] Author to whom any correspondence should be addressed.

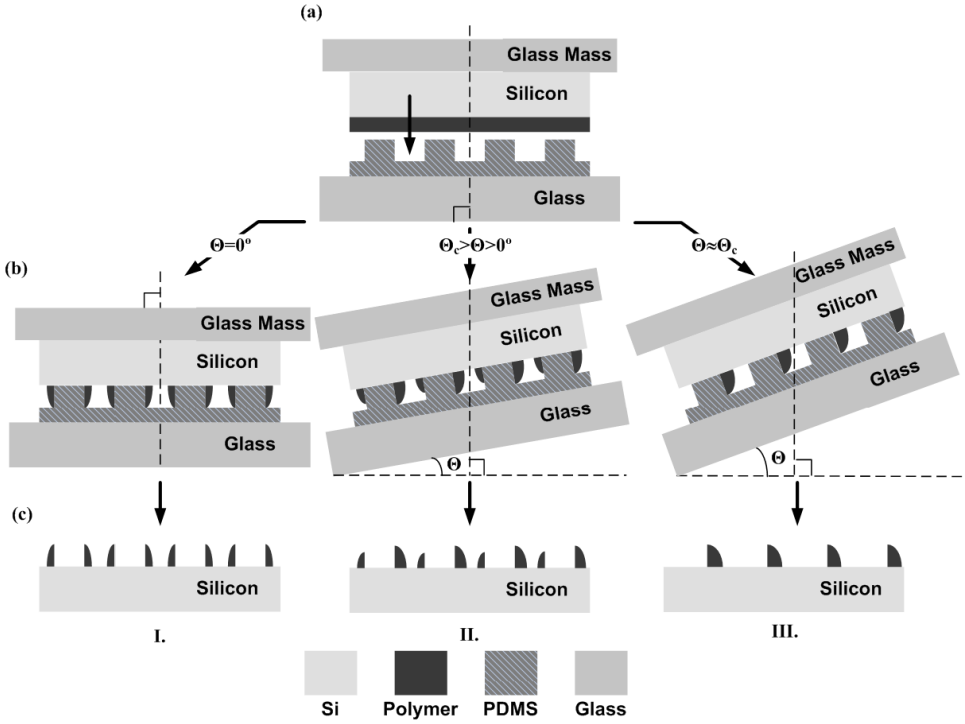

Figure 1. Schematic illustration of the INIL fabrication process for (I) $\theta = 0°$; (II) $0° < \theta < \theta_c$ (≈5°); (III) $\theta \approx \theta_c$ (≈5°).

of NIL and soft lithography, but also removes the need for either nanoscale 3D templates or precise template-to-substrate alignment. Various nanoscale devices can be envisaged by exploiting INIL, including angle-resolved photonic crystals and anisotropic 'smart' surfaces.

2. Fabrication

2.1. Experimental details

Figure 1 schematically illustrates the INIL fabrication process. A PDMS stamp (approximately 1 cm × 1 cm) is initially created with a desired micropattern by casting and curing PDMS prepolymer (Sylgard 184, Dow Corning, 60 °C for 24 h) on a silicon master template patterned by conventional photolithography (or electron-beam lithography) followed by a plasma dry etching procedure. Various micropatterns have been investigated, such as trenches (1 μm in width, 1 μm in depth, and 2 μm in lateral pitch separation) with overall pattern areas (width × length) ranging from 100 μm × 1 mm to 500 μm × 3 mm; square columns (1 μm in width and 2 μm in lateral pitch separation); and cylindrical pillars (1 μm in diameter, 1 μm in depth and 2 μm in lateral pitch separation) with overall pattern areas ranging from 100 μm × 100 μm to 500 μm × 500 μm for both. The PDMS stamp is then treated by O_2 plasma (1 min) for surface energy enhancement and brought into contact with a silicon substrate (approximately 1 cm × 1 cm) bearing a thin ZEP520 film (30–50 nm), and intimate contact is maintained by applying a glass plate to the top surface (figure 1(a)). The entire assembly is then inclined at a small angle θ, typically between 0° and 5°, and annealed at a temperature above the ZEP520 glass transition temperature (T_g = 105 °C) for several hours, e.g. 12 h in vacuum at 170 °C. During the annealing, the polymer flows and tends to dewet from the Si substrate, preferentially wetting the PDMS sidewalls. When $\theta = 0°$ (figure 1-I), this dewetting–wetting process results in symmetric polymer flow, and consequently a symmetric polymer pattern profile with nanometer feature sizes of the same height is produced (figure 1-I(b)). This nanopattern is revealed by cooling the assembly to room temperature and removing the PDMS stamp (figure 1-I(c)). Using a mold consisting of parallel trenches results in a regular pattern of lines that have a 1 μm pitch but with much smaller dimensions than the trench patterns in the PDMS stamp. For example, for a film of initial thickness of 30 nm the resulting line height at 0° inclination angle is approximately 100 nm and the full width half maximum (FWHM) of the lines is approximately 300 nm, as shown in figure 2(a). This is equivalent to the dewetting process reported by Zhang *et al* [8]. Increasing θ from 0° consequently leads to asymmetric wetting–dewetting behavior of the polymer flow (figure 1-II), and as a result 3D nanoline patterns with different heights and widths are obtained (figure 1-II(c)). When θ is increased to close to or beyond a threshold angle θ_c, which is approximately equal to 5°, wetting only occurs on one face of the PDMS (figure 1-III(b)); therefore the profile evolves to produce only one nanoline per pitch spacing (figure 1-III(c)).

2.2. Results and discussion

Figure 2 shows AFM images of the resulting 3D nanolines produced by INIL at different values of θ in an initial approximately 30 nm thick ZEP520 polymer layer. Different feature heights are obtained when the inclination angle is

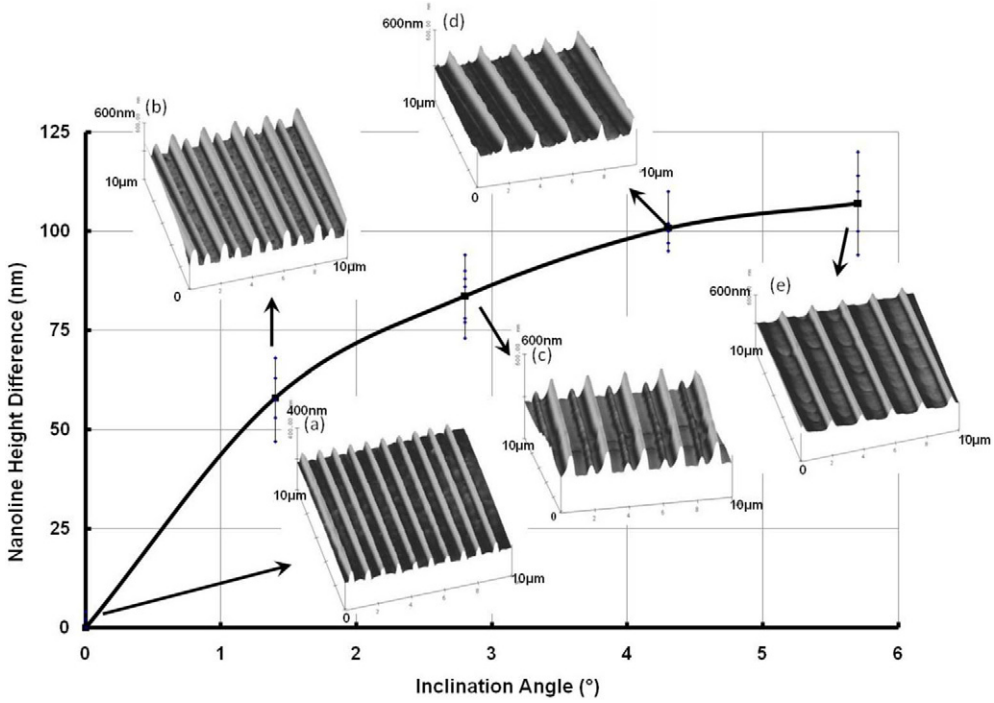

Figure 2. Plot of nanoline height difference as a function of inclination angle (the polymer film thickness y is 30 nm). The inserted AFM images in the 3D views are the resulting 3D nanolines with different heights at various θ: (a) $\theta = 0°$ (z scale bar = 400 nm); (b) $\theta = 1.4°$ (z scale bar = 600 nm); (c) $\theta = 2.8°$ (z scale bar = 600 nm); (d) $\theta = 4.3°$ (z scale bar = 600 nm); (e) $\theta = 5.7°$ (z scale bar = 600 nm). The x–y area in all AFM images is 10 μm × 10 μm.

varied from 0° to 5°. The height of the symmetric nanoline (figure 2(a)) is 100 nm, and the full width half maximum (FWHM) of the lines is 300 nm. Comparison of the volumes of the polymer film patterns before and after INIL indicates that there is volume conservation between the non-patterned polymer thin film before INIL and the resulting polymer nanopattern. Therefore the entire polymer mass is also conserved without any loss in the INIL process. For asymmetric nanolines (figures 2(b)–(e)) the height and width are dependent on the inclination angle, but the total volume of polymer is still conserved.

In order to understand the effect of the inclined angle, the measured nanoline height difference Δh is plotted as a function of the inclination angle θ shown in figure 2. These data show that under the same experimental conditions the height difference of the nanolines is primarily dependent on the magnitude of the inclination angle θ. When θ is close to or above 5°, the height difference Δh saturates and the extreme asymmetric structure is obtained (figure 2(e)).

The effect of the initial thin film thickness on the resulting nanoline height difference was studied, using two polymer films of thicknesses equal to 30 nm and 50 nm respectively. The line height differences obtained from these two series, Δh_{30} and Δh_{50}, are plotted and compared in figure 3 as a function of the inclination angle. It is clear that the 50 nm film produces a larger nanoline height difference than the 30 nm film at the same inclination angle, $\Delta h_{50} > \Delta h_{30}$. In other words, the 50 nm film requires a smaller magnitude of the inclined angle than 30 nm film does in order to obtain the same Δh. Moreover, the difference in Δh between the two

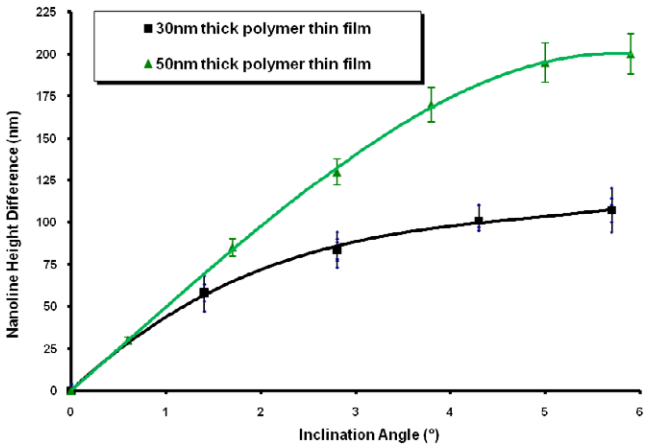

Figure 3. Plots of nanoline height differences as a function of the inclination angle θ produced in (■) 30 nm and (▲) 50 nm ZEP520 thin films, respectively, by INIL.

films ($\Delta h_{50} - \Delta h_{30}$) increases with increasing θ. When θ is approximately equal to 5°, the height differences of both series of films reach their maximal values, $\Delta h_{50\,\max}$ and $\Delta h_{30\,\max}$, and the extreme asymmetric structures appear respectively. The ratio of $\Delta h_{50\,\max}$ to $\Delta h_{30\,\max}$ is approximately the same as the ratio of the original film thicknesses. These observations indicate that the resulting 3D nanostructure can be influenced by the initial film thickness.

Moreover, other 3D shapes have also been successfully demonstrated by INIL, such as symmetric and asymmetric nanocircles by using a cylindrical pillar PDMS stamp, as

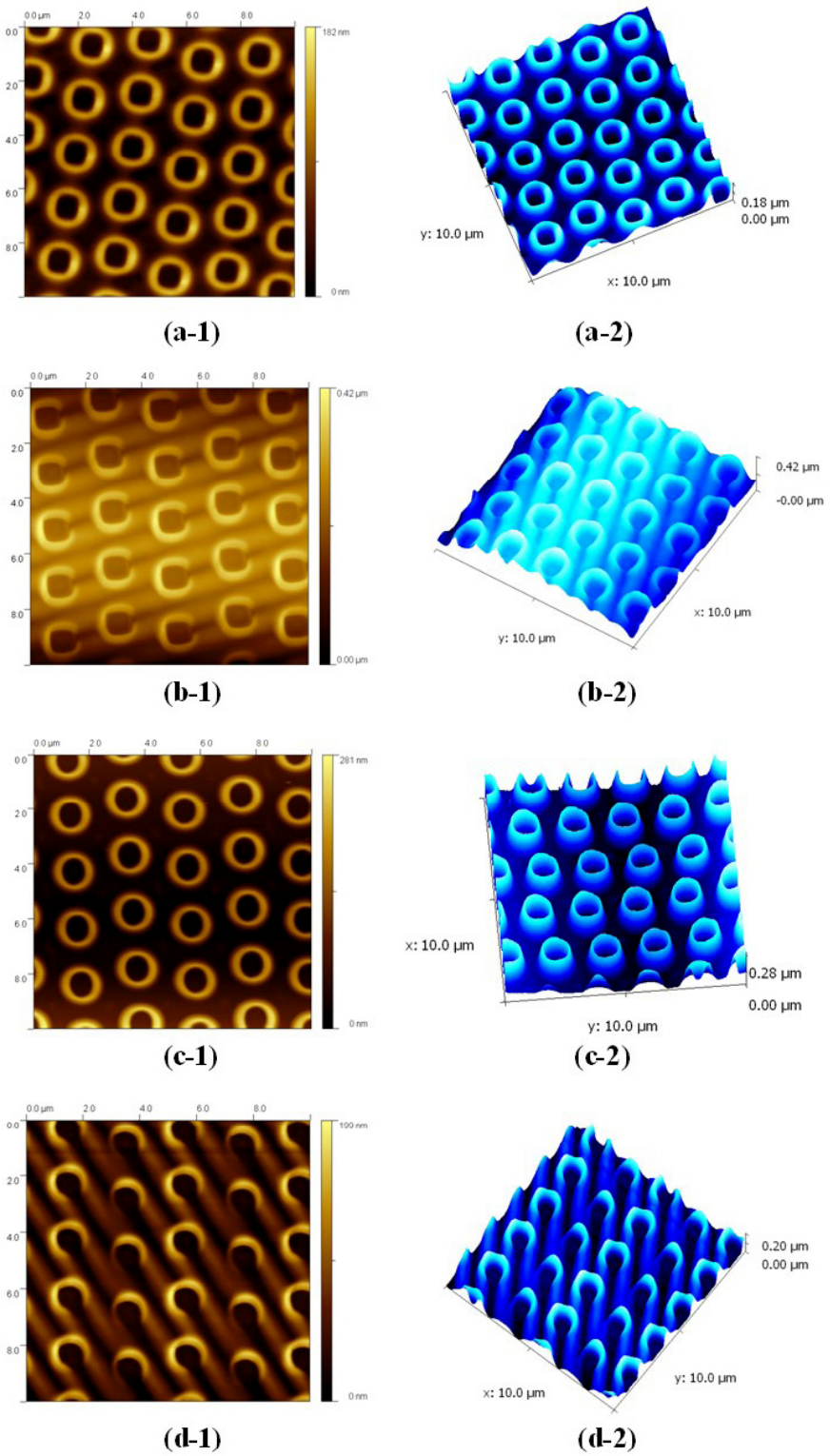

Figure 4. AFM images of the resulting nanosquares and nanocircles produced by INIL in 2D (left) and 3D (right) views: (a-1) and (a-2), symmetric nanosquares (z scale bar = 180 nm); (b-1) and (b-2), asymmetric nanosquares (z scale bar = 420 nm); (c-1) and (c-2), symmetric nanocircles (z scale bar = 280 nm); (d-1) and (d-2), asymmetric nanocircles (z scale bar = 200 nm). The x–y area in all AFM images is 10 μm × 10 μm.

well as symmetric and asymmetric nanosquares, as shown in figure 4. It can be observed that the corners of the resulting nanosquares are rounded. This could be attributed to the PDMS mold that is unable to hold sharp 90° corners due to the material properties. This can be potentially addressed by using a rigid mold with proper 90° corners.

Although uniformity was not quantitatively assessed, visual inspection indicated no significant uniformity variation over the entire pattern dimension (100 μm × 1 mm to 500 μm × 3 mm for nanolines, and 100 μm × 100 μm to 500 μm × 500 μm for both nanocircles and nanosquares). Uniformity of very large pattern areas, such as over the extent of a 4 inch wafer, should be possible by ensuring uniform application of a sufficient and suitable force (F_{mass}) over the overall pattern area, e.g. using a properly designed INIL setup.

3. Study of the mechanism

In general, the dewetting phenomenon of polymer thin films can be explained by analyzing the free energy of the system [13, 15, 16]. The simplest systems are uniform thin films on horizontally flat surfaces. Dewetting leads to a film morphology change, e.g. into droplets or other patterns. When a PDMS mold with topographic features is introduced to the system, the film is consequently in contact with two different surfaces, the mold and the substrate, and tends to reach the system equilibrium, minimum free energy, deforming in a three-dimensional frame. An example is the resulting uniform 3D nanopatterns of the same height reported by Zhang *et al* [8].

It is clear that 3D nanopatterns result from a balance of the different forces and energies experienced by the polymer as it interacts with two different surfaces: the silicon substrate and the PDMS sidewall. Although energy arguments are important in determining the ultimate dewetting state of the polymer, the kinetics associated with the transition to this ultimate state must also be considered, especially for these viscous polymers. Therefore to understand the INIL mechanism it is important to analyze the forces and the process from the kinetics point of view.

The formation of 3D nanostructures in INIL is a dynamic process. It includes movement of the polymer that is initially in contact with and underneath the PDMS stamp into the cavity followed by wetting the PDMS sidewalls to minimize the system surface energy. The polymer in the PDMS cavity (not in contact with PDMS stamp) simultaneously dewets the Si substrate (and wets the PDMS sidewalls) during annealing to minimize the system surface energy. It was observed that dewetting of a ZEP520 thin film (50 nm) from a Si substrate without a PDMS stamp started within 15 min at 170 °C, forming small holes, and reached equilibrium within a time scale of approximately 2 h, similar to polystyrene thin films (80 nm) dewetting at 135 °C [18]. The film dewetting time is apparently shorter than the INIL process completion time obtained at 170 °C. This indicates that movement of the polymer underneath the PDMS is likely the limiting step affecting the INIL process completion time. The forces of interest in INIL consist of the wetting and dewetting forces associated with the PDMS mold and silicon substrate surface respectively, as well as the force $F_{\text{mass}} = mg$ exerted on the polymer film due to the total mass of glass and silicon acting on the polymer (m). The gravitational body force of the polymer thin film itself is several orders of magnitude smaller than F_{mass} and can therefore be neglected.

When $\theta = 0°$, the symmetric wetting and dewetting forces result in 3D nanopatterns with the same height, as demonstrated in our results, as well as the work of Zhang *et al* [8]. In [8] the PDMS mold is placed onto the polymer thin film spin-coated on a substrate, which can be likened to an 'inverted' INIL process ($\theta = 0°$). Zhang *et al* have demonstrated that the wetting and dewetting forces lead the polymer to flow in the opposite direction relative to gravity. This observation confirms that the gravitational force of the polymer thin film itself is negligible compared to the wetting force. We also studied and compared this 'inverted' INIL process ($\theta = 0°$) to the standard INIL process. The annealing time and temperature are identical to those for the INIL structure. We observed that the INIL structure shows clear separation between the dewetting lines (figure 2(a)), which does not occur in the 'inverted' INIL case. However, if the 'inverted' INIL example is annealed for a longer time at a higher temperature, a structure that closely resembles figure 2(a) is observed. Clearly, inverting the system does not affect the ultimate structural form, but does affect the kinetic behavior of the polymer. The difference is attributed to the larger normal force (F_{mass}) in INIL induced by the top glass and silicon acting on the polymer (figure 5(a)). This force is greatly reduced in the 'inverted' INIL case; therefore a longer time scale at a higher temperature and lower polymer viscosity is required to reach a given state. Increase of the normal force or normal pressure may increase the movement rate, but deformation of the PDMS stamp can occur at high normal forces, so it is not always practical to simply increase the normal force or pressure. The same concern is present in the case when the inclination angle θ is above 0°.

When θ is above 0° (figure 5(b)), F_{mass} generates both a lateral shear on the polymer ($F_{\text{mass}} \sin\theta$) and a normal force ($F_{\text{mass}} \cos\theta$) pressing the polymer thin film for relocation. The magnitudes of these two forces are dependent on the inclination angle, while the wetting or dewetting force is not affected by the inclination angle. When θ is very small or close to 0°, $F_{\text{mass}} \sin\theta$ is negligible, and thus the wetting/dewetting forces and $F_{\text{mass}} \cos\theta$ are the primary forces influencing the movement of the polymer. As θ increases from 0°, a shear force $F_{\text{mass}} \sin\theta$ becomes significant and a shear-force-driven mechanism is also present that induces asymmetric movement of the polymer under the stamp. Consequently, more polymer material builds up on one of the PDMS mold walls compared to the other.

When imposing this angle-dependent shear force onto the polymer in this INIL configuration, it is possible to derive the time (t) taken for the polymer with a viscosity of $\eta(T)$ to move a distance (d) at an average velocity ($\bar{v} = d/t$). Assuming the polymer to act as Newtonian fluid in the INIL process, the average shear stress (τ) is proportional to the strain rate ($\dot{\gamma}$) where the polymer viscosity ($\eta(T)$) is the constant factor of proportionality as shown in equation (1). The average shear stress (τ) applied to the fluidic polymer thin film can be equated to the force load ($mg \sin\theta$) per cross-section area (A) as shown in equation (2).

$$\tau = \eta(T)\dot{\gamma} \doteq \eta(T)\frac{\bar{v}}{y} = \eta(T)\frac{d}{yt}, \tag{1}$$

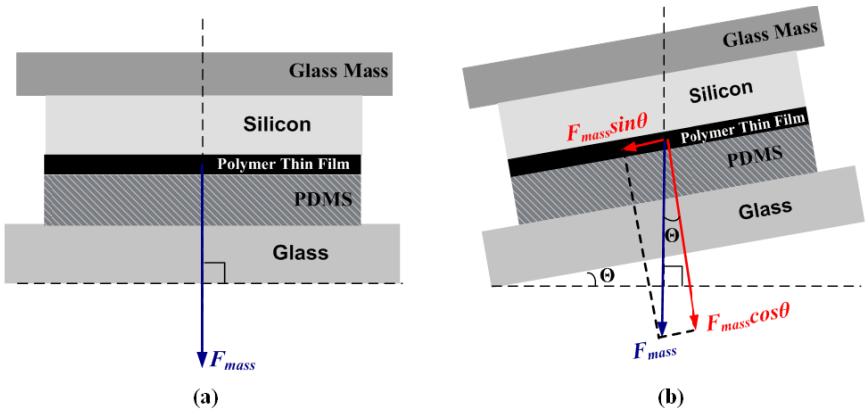

Figure 5. Schematic illustration of the assembly in the INIL process for (a) $\theta = 0°$, and (b) $\theta > 0°$.

where y is the polymer film thickness, $\eta(T)$ is the polymer viscosity and can be obtained from the empirical Williams–Landel–Ferry (WLF) model as shown in equation (3).

$$\tau = \frac{mg\sin\theta}{A}, \tag{2}$$

where g is the gravitation constant equal to 9.8 m s^{-2}.

$$\eta(T) = \eta_0 \exp\left[\frac{-C_1(T - T_r)}{C_2 + T - T_r}\right], \tag{3}$$

where T is the experimental temperature, T_r is the reference temperature chosen as 148 °C, η_0 is the zero-shear viscosity, $C_1 = 8.86$ and $C_2 = 101.6$ K [17]. The value of η_0 for the ZEP polymer at T_r (=148 °C) was measured using a rotational rheometer with parallel-plate geometry and is equal to 3.2×10^5 Pa s.

$$t \approx \frac{dA}{ymg\sin\theta}\eta(T). \tag{4}$$

The magnitude of t can be derived by rearranging equations (1)–(3). When d is equal to the distance between the PDMS's two nearest sidewalls, e.g. the 1 μm width of the PDMS pattern in contact with the polymer layer, the calculated t would represent the INIL process time. According to equations (3) and (4) a relationship between INIL process time (t) and annealing temperature (T) can be determined, as shown in the solid curve in figure 6, where the parameters are set as $d = 1 \times 10^{-6}$ m, $A = 1 \times 10^{-4}$ m^2, $y = 5 \times 10^{-8}$ m, $m = 7$ g and $\theta = 3°$.

Figure 6 also shows the values of $t(T)$ (●) obtained experimentally ($T = 150$, 170, 210, 230 °C) by examining a series of samples prepared and processed using a PDMS trench stamp with a feature size $d = 1 \times 10^{-6}$ m, polymer-coated silicon substrate area $A = 1 \times 10^{-4}$ m^2, thin film thickness $y = 5 \times 10^{-8}$ m, applied mass $m = 7$ g and an inclination angle $\theta = 3°$. The actual INIL process time at each temperature of interest is obtained by characterizing the nanoline pattern at different time intervals of the INIL process, e.g. 0.5, 2, 8, 12 h, until the time when complete nanoline patterns are observed, as illustrated in figure 7. Each data point obtained in figure 6 is averaged from five samples. The vertical

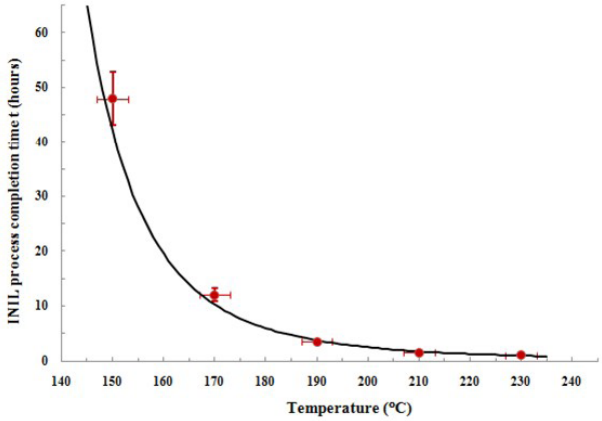

Figure 6. Plot of INIL process time as a function of process temperature, $t(T)$, for $\theta = 3°$: (–) theoretical and (●) experimental data. The vertical error bars represent the maximum and minimum measurement values of five samples at each temperature point.

error bars represent the maximum and minimum time values achieved. It is clear that the experimental data fit the theoretical $t(T)$ model very well, especially when the temperature is above 170 °C. The difference observed in the low temperature region (e.g. $T = 150$ °C) is most probably associated with the relatively high viscosity where the polymer properties diverge from Newtonian behavior, leading to discrepancies between the experimental and the estimated data. Also, it was observed that the resulting nanopatterns at low annealing temperature were wider and shorter (smaller height) than the patterns produced at high annealing temperatures due to the higher viscosity of the polymer and the slower dewetting/wetting rates at low annealing temperatures. Significantly increasing the process time might result in nanopatterns analogous to the ones produced at high annealing temperatures. It is hypothesized that the process completion time at low annealing temperatures ($T < 150$ °C) can be limited by polymer dewetting/wetting or a combination of polymer dewetting and its movement to the PDMS cavity in INIL.

In this study, the developed INIL model provides important information allowing evaluation of the INIL process, and assists in establishing the design parameters for the desired 3D structures. Such design parameters include the PDMS

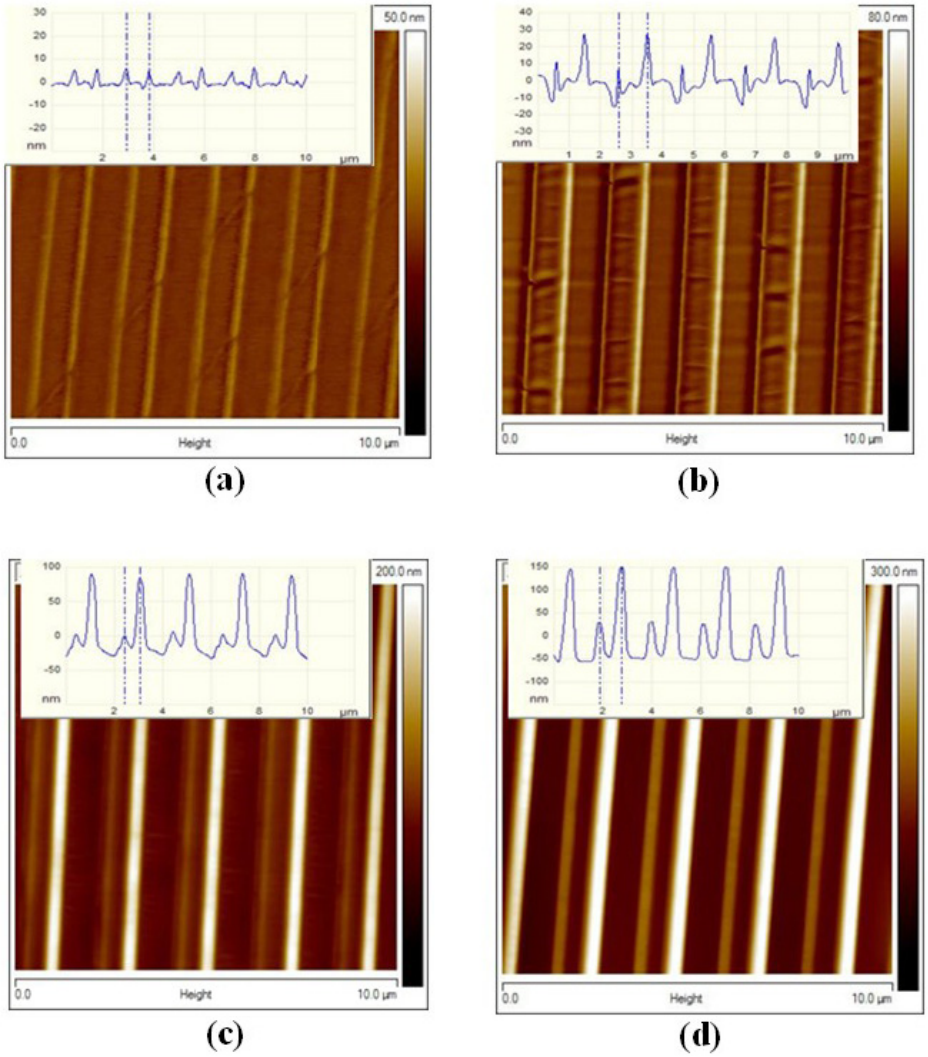

Figure 7. AFM images of the nanolines obtained at different time intervals ($A = 1 \times 10^{-4}$ m^2, $y = 5 \times 10^{-8}$ m, $m = 7$ g, $\theta = 3°$, $T = 170\,°$C). The inserted images are representative AFM section analyses respectively. (a) 0.5 h, $\Delta h = 0$, (b) 2 h, $\Delta h = 30 \pm 5$ nm, (c) 8 h, $\Delta h = 85 \pm 5$ nm, (d) 12 h, $\Delta h = 120 \pm 10$ nm. The x–y area in all AFM images is 10 μm $\times$ 10 μm.

stamp width (d), the film thickness (y), the inclined angle (θ), the applied mass (m), the process temperature (T) and the polymer material properties (T_g and $\eta(T)$). Although this work is focused on the micron or sub-micron nanopattern separation distance, it is feasible in theory to fabricate 3D nanopatterns with sub-100nm separation distances by using a sub-100 nm patterned PDMS stamp [19] ($d \leqslant 100$ nm) and also reducing the initial polymer film thickness to 5–10 nm. Smaller film thicknesses would allow polymer dewetting at smaller length scales. On the other hand, use of the INIL technique using sub-100 nm mold feature sizes must include strategies to ensure intimate contact between the stamp and substrate without deforming the small PDMS stamp features as well as to remove the adhesion issue in the stamp–substrate separation step.

4. Conclusion

In this paper, inclined nanoimprinting lithography (INIL) has been demonstrated. The capability of fabricating 3D nanostructures of varying heights over large surface areas on the planar substrate in a single step is achieved. The underlying INIL mechanism has been investigated and compared to experimental results. The analysis of experimental results indicates that the angle-dependent 3D nanostructure produced in INIL is due to the mass-generated force incident on the polymer film induced by the INIL apparatus when the inclined angle is greater than zero. Various 3D nanoscale devices and structures can be envisaged by INIL in photonics/plasmonics, nanotribology and NEMS, including angle-resolved photonic/plasmonic crystals and anisotropic functional surfaces.

Acknowledgments

The authors would like to thank Dr Seong-Hyok Kim, Mr Ryan Kincer and Mr Wei Zhang for the technical help and discussion in this work.

References

[1] Chen Y and Pépin A 2001 *Electrophoresis* **22** 187–207
[2] Chou S Y, Keimel C and Gu J 2002 *Nature* **417** 835–7
[3] Chou S Y, Li W-D and Liang X 2009 *Nanotechnology* **20** 155303
[4] Guo L J 2007 *Adv. Mater.* **19** 495–513
[5] Ahn S, Cha J, Myung H, Kim S M and Chang S 2006 *Appl. Phys. Lett.* **89** 213101
[6] Gates B D, Xu Q B, Love J C and Whitesides G M 2004 *Annu. Rev. Mater. Res.* **34** 339–72
[7] Jeon S, Menard E, Park J U, Maria J, Meitl M, Zaumseil J and Rogers J A 2004 *Adv. Mater.* **16** 1369–73
[8] Zhang H L, Bucknall D G and Dupuis A 2004 *Nano Lett.* **4** 1513–9
[9] Zaumseil J, Meitl M A, Hsu J W P, Acharya B R, Baldwin K W, Loo Y L and Rogers J A 2003 *Nano Lett.* **3** 1223–7
[10] Zhao Y Z, Yoon Y K, Choi S O, Wu X S, Liu Z and Allen M G 2009 *Appl. Phys. Lett.* **94** 023301
[11] Yu Q, Braswell S, Christin B, Xu J, Wallace P M, Gong H and Kaminsky D 2010 *Nanotechnology* **21** 355301
[12] Liu Z, Bucknall D G and Allen M G 2007 *Proc. Transducers 2007: 14th Int. Conf. on Solid-State Sensors, Actuators and Microsystems (Lyon)* pp 1621–4
[13] Bucknall D G 2004 *Prog. Mater. Sci.* **49** 713–86
[14] Medeiros D R, Aviram A, Guarnieri C R, Huang W S, Kwong R, Magg C K, Mahorowala A P, Moreau W M, Petrillo K E and Angelopoulos M 2001 *IBM J. Res. Dev.* **45** 639–50
[15] Reiter G 1993 *Langmuir* **9** 1344–51
[16] Leopoldes J, Dupuis A, Bucknall D G and Yeomans J 2003 *Langmuir* **19** 9818–22
[17] Aoki Y and Tanaka T 1999 *Macromolecules* **32** 8560–5
[18] Seemann R, Herminghaus S, Neto C, Schlagowski S, Podzimek D, Konrad R, Mantz H and Jacobs K 2005 *J. Phys.: Condens. Matter* **17** S267–90
[19] Odom T W, Love J C, Wolfe D B, Paul K E and Whitesides G M 2002 *Langmuir* **18** 5314–20